NANO LETTERS

2007
Vol. 7, No. 5
1419−1423

# A Paramagnetic Nanoprobe To Detect Tumor Cell Death Using Magnetic Resonance Imaging

**André A. Neves,[†] Anant S. Krishnan,[†] Mikko I. Kettunen,[†] De-en Hu,[†] Maaike M. de Backer,[†] Bazbek Davletov,[‡] and Kevin M. Brindle*,[†]**

*Department of Biochemistry, University of Cambridge, Tennis Court Road, Cambridge CB2 1GA, U.K., and Neurobiology Division, MRC Laboratory of Molecular Biology, Hills Road, Cambridge CB2 2QH, U.K.*

*Received January 17, 2007; Revised Manuscript Received March 6, 2007*

**ABSTRACT**

**A 110 kDa (ca. 5 nm in diameter) bivalent paramagnetic nanoprobe for detecting cell death using magnetic resonance imaging (MRI) is described, in which two biotinylated C2A domains of the protein synaptotagmin-I were complexed with a single avidin molecule, which had been labeled with gadolinium chelates. This nanoprobe bound with high affinity and specificity to the phosphatidylserine exposed by dying cells and was demonstrated to allow MRI detection of apoptotic tumor cells in vitro.**

The efficacy of conventional and novel tumor therapies is still largely evaluated using methods introduced more than 20 years ago, in which response to therapy is determined from measurements of tumor size.[1,2] However, evidence of tumor shrinkage may take weeks to become manifest and, for some tumor therapies, there may be only arrest of tumor growth rather than the induction of full tumor regression. Therefore the development of sensitive and specific non-invasive imaging methods that can give an early indication of tumor response to treatment has become a major area of research.[3]

Positron emission tomography (PET) measurements of the reduction in ($^{18}$F)-fluoro-2-deoxy-D-glucose (FDG) uptake are now widely used for the detection of tumor responses to treatment in the clinic[4] and have been shown to be effective for assessing response in specific tumor types, in particular lymphoma[5] and lung cancer.[6] $^{99m}$Tc-labeled annexin V (AnxV), which binds to phosphatidylserine (PS) on the surface of apoptotic cells, has also been used in the clinic as an imaging agent for detecting tumor cell death post-treatment.[7,8] The resolution of these radionuclide imaging techniques, however, is low (3−7 mm for PET in clinical practice[9]) when compared to magnetic resonance imaging (MRI); the techniques involve exposure of the patient to ionizing radiation and, in the case of FDG, requires the production of a relatively expensive and short-lived labeled compound. There has, therefore, been interest in the development of MRI methods for detecting response to cancer therapy. These can produce images of comparatively high resolution, do not involve ionizing radiation, and may employ targeted contrast media that should be relatively inexpensive to produce.[10]

The 14 kDa C2A domain of synaptotagmin I, like AnxV, binds in a $Ca^{2+}$-dependent manner and with nanomolar affinity to PS externalized on the surface of dying cells. We showed previously that, when conjugated to superparamagnetic iron oxide (SPIO) nanoparticles, C2A could be used to detect apoptosis using MRI, both in vitro and in vivo, in a tumor treated with chemotherapeutic drugs.[11,12] Although sensitive to detection by MRI, the negative contrast that SPIO nanoparticles produce can make them difficult to detect in the pre-existing irregular, heterogeneous, and time varying contrast found in tumors. Furthermore, the large size of these reagents (in the tens-to-hundreds of nanometers range) can impede extravasation of the nanoprobe from the tumor microvasculature and can also limit subsequent clearance of unbound material and hence the generation of specific tissue contrast. This is an important issue for any tumor-targeting agent.[13] We have, therefore, been developing targeted agents in which C2A is conjugated to $Gd^{3+}$ chelates.[11] These are much smaller than the SPIO agents (typically 5−10 nm) and give positive contrast in $T_1$-weighted images, which should make them easier to detect. We showed previously that the very strong binding of avidin to biotin could be exploited to attach biotinylated C2A to a $Gd^{3+}$-chelate-labeled avidin, the latter thus serving as a generic MRI-detectable label, in a two-step imaging approach.[11] We describe here a smaller,

* Corresponding author. E-mail: kmb@mole.bio.cam.ac.uk. Tel: +44 (0) 1223 333674. Fax: +44 (1)1223 766002.
† Department of Biochemistry, University of Cambridge.
‡ Neurobiology Division, MRC Laboratory of Molecular Biology.

10.1021/nl070126v CCC: $37.00 
**Published on Web 04/06/2007**

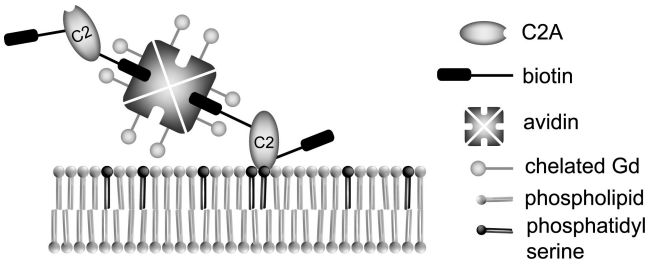


**Figure 1.** Schematic representation of a $[biotC2]_2$[Avidin-Gd] nanoprobe binding to phosphatidylserine (PS) externalized on the surface of apoptotic cells.

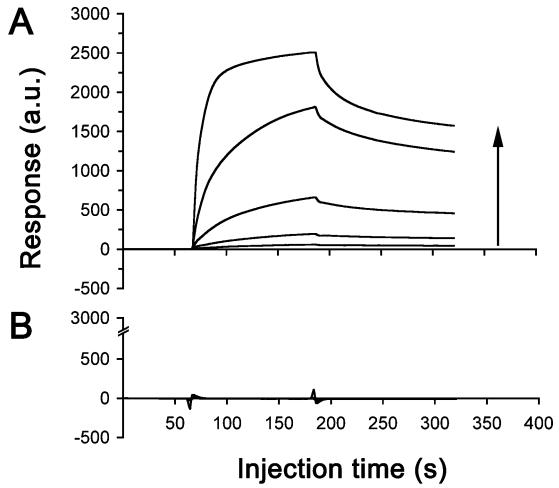


**Figure 2.** Representative surface plasmon resonance (SPR) sensorgrams (relative response vs time) of active (A) and inactive (B) $[biotC2A]_2$[Avidin-Gd] nanoprobes binding to PS. A L1 sensor chip was coated with PS-containing liposomes, and the proteins were injected, in $Ca^{2+}$-containing buffer, at increasing concentrations (see arrow, active: 7.3, 29.3, 117, 469, 1875 nM; inactive: 4.9, 19.5, 78.1, 313, 1250 nM). Each sample was injected in triplicate at 25 °C. Response was proportional to the concentration of the active bivalent nanoprobe (A). No significant response was detected for the inactive nanoprobe at any concentration (B). Abbreviation: a.u., arbitrary units.

single-component, and bivalent avidin-based nanoprobe (Figure 1), which shows greater specificity for binding to dying cells, increased affinity for PS, and a greater capability to generate positive contrast in the MR image.

Recombinant C2A and a site-directed mutant (D230N) of C2A ((i)C2A) that was inactive in PS binding and which served as a control were expressed in *E. coli* and purified by affinity chromatography (see Supporting Information). The proteins were biotinylated on their lysine $\epsilon$-amino groups using the *N*-hydroxysulfosuccinimide (NHS) ester of biotin (sulfo-NHS-LC-biotin, Pierce Biotechnology, Rockford, IL) and shown to have two to three biotin moieties attached, as determined by mass spectrometry (MALDI-TOF, TofSpec 2E instrument, Waters, Milford, MA) and by the HABA ((2-(4′-hydroxyazobenzene)benzoic acid) spectrophotometric assay (Pierce Biotechnology).[14] Protein that had been inactivated by biotinylation was removed by affinity chromatography. Active biotinylated C2A had a similar dissociation constant for binding to PS ($K_d \sim 20$ nM) as the unmodified protein (data not shown). This dissociation constant is approximately

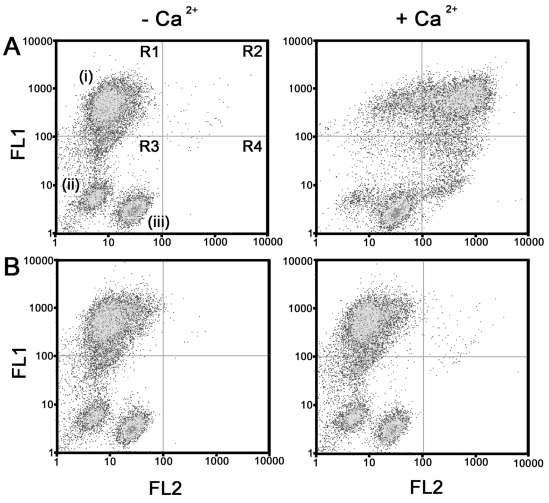


**Figure 3.** Flow cytometric analysis of the binding of active (A) and inactive (B) $[biotC2A]_2$[Avidin-Gd] nanoprobes, to apoptotic EL-4 cells, in the absence ($-Ca^{2+}$) and presence ($+Ca^{2+}$) of calcium. Binding of the nanoprobes was detected using NeutrAvidin-Alexa-350 ($\lambda_{ex} = 346$; $\lambda_{em} = 442$ nm, FL2-axis). Necrotic cells were detected using propidium iodide, PI ($\lambda_{ex} = 535$; $\lambda_{em} = 617$ nm, FL1-axis). Dual-scatter plots of these two parameters are shown. (i) necrotic cell population; (ii) apoptotic cell population; (iii) viable cell population. $-Ca^{2+}$, cells were incubated in Hepes-buffered saline (HBS) containing 10 mM EDTA; $+Ca^{2+}$, cells were incubated in HBS containing 2 mM $Ca^{2+}$.

5-fold lower than the dissociation constant of the GST-tagged derivative of the protein that was used previously.[11,12]

An avidin-[Gd-DTPA] conjugate was prepared by reacting avidin (Affiland, Liege, Belgium) with the chelating agent 2-(4-isothiocyanatobenzyl)-6-diethylenetriaminepentaacetic acid (*p*-SCN-Bn-DTPA) (Macrocyclics, Dallas, TX), using a modified version of a protocol described previously.[11] The number of Gd-DTPA molecules conjugated to avidin was estimated, using MR T1 measurements on the $Gd^{3+}$ released by strong acid treatment, at 15−20 mol of $Gd^{3+}$ per mole of protein, with no significant loss of biotin-binding activity. The spin lattice ($r_1$) and spin−spin ($r_2$) relaxivities of [Avidin-Gd] were $95 \pm 5$ $mM^{-1}$ $s^{-1}$ and $987 \pm 24$ $mM^{-1}$ $s^{-1}$, respectively, at 9.4 T.

The [Avidin-Gd] conjugate was complexed with active and inactive biotinylated C2A (biotC2A and biot-(i)C2A) at different molar ratios to prepare complexes with stoichiometries in the range of 1-[Avidin-[Gd-DTPA]] to 4-[biot-C2A]. The $r_1$ and $r_2$ relaxivities of the bivalent complexes, $[biotC2A]_2$.[Avidin-Gd] and $[biot\text{-}(i)C2A]_2$[Avidin-Gd], were in the ranges 170−190 and 1800−1900 $mM^{-1}$ $s^{-1}$, respectively, at 9.4 T. This complexation, which increased the mass of the [Avidin-Gd] by a factor of 1.4, produced a substantial (1.9-fold) increase of the $r_1$ and $r_2$ relaxivities. This may be due, at least in part, to the increase in the rotational correlation time of the bivalent complexes.[15,16] The bivalent, $[biotC2A]_2$.[Avidin-Gd] complex had a 3-fold higher $r_1$ relaxivity compared to the GST-C2A−avidin complex described previously (175 $mM^{-1}$ $s^{-1}$ vs 60 $mM^{-1}$ $s^{-1}$, at 9.4 T[11]), reflecting an increased degree of modification of the avidin with $Gd^{3+}$ chelates.

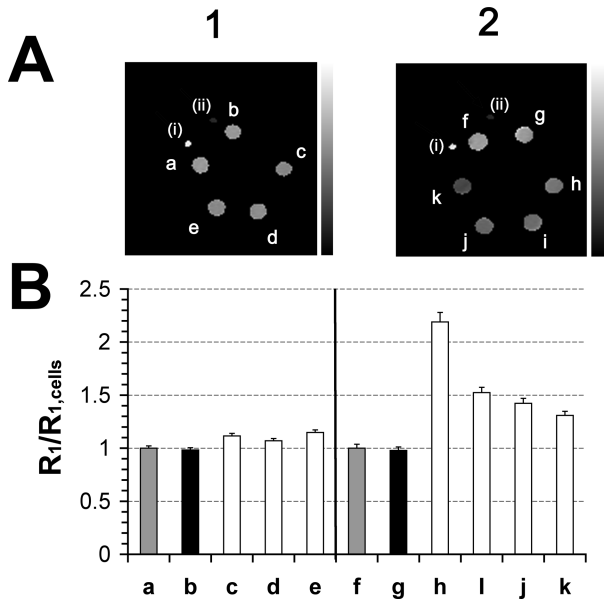


**Figure 4.** Relative $T_1$ relaxation times of active [biotC2A]$_n$[Avidin-Gd] complexes bound to apoptotic EL-4 cells. The images shown in (A) are maps of the $T_1$ relaxation times obtained from cell samples. The $T_1$ relaxation rates ($1/T_1$) obtained from these images ($R_1$, mean ± SD) are shown in (B), expressed as a ratio relative to the mean $R_1$ value for apoptotic cells (tube a for the two-step method and tube f) for the one-step method). A two-step addition of biotC2A, followed by [Avidin-Gd] (1) was compared with (2) a one-step addition of the nanoprobe prepared with different molar ratios of biotC2A to [Avidin-Gd], in the range 0.8−3.0. In the two-step method (1), apoptotic cells ($10^7$) were incubated at 20 °C, in HBS containing 2 mM $Ca^{2+}$, with (c) 100 $\mu$M biotC2A, 60 $\mu$M [Avidin-Gd], $n = 1.7$; (d) 50 $\mu$M biotC2A, 60 $\mu$M [Avidin-Gd], $n = 0.8$; (e) 30 $\mu$M biotC2A, 60 $\mu$M [Avidin-Gd], $n = 0.5$; and in the one-step method (2) with (h) 72.8 $\mu$M biotC2A, 24.0 $\mu$M [Avidin-Gd], $n = 3$; (i) 36.4 $\mu$M biotC2A, 24.0 $\mu$M [Avidin-Gd], $n = 1.5$; (j) biotC2A 18.0 $\mu$M, [Avidin-Gd] 24.0 $\mu$M, $n = 0.8$; (k) 9.2 $\mu$M biotC2A, 12.0 $\mu$M [Avidin-Gd], $n = 0.8$. Following incubation with the nanoprobes, the cells were then washed and imaged. Tubes a and f contained apoptotic cells alone and tubes b and g apoptotic cells that had been incubated with 60 $\mu$M [Avidin-Gd] alone. The two capillaries (i, ii) were used as references and contained buffer and 60 $\mu$M [Avidin-Gd], respectively. *n* represents the molar ratio of biotC2A to [Avidin-Gd]. The gray scale in (A) represents $T_1$ relaxation time (0−3 s).

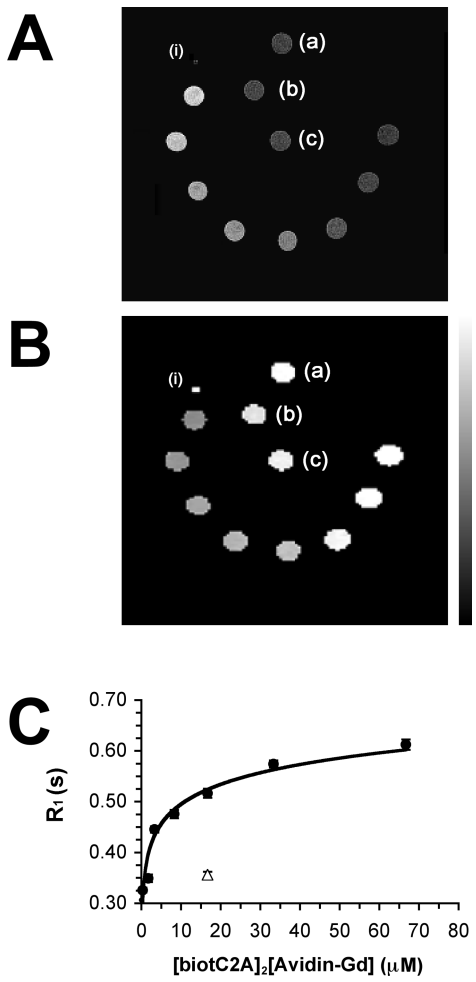


**Figure 5.** $T_1$ relaxation times for the active [biotC2A]$_2$[Avidin-Gd] nanoprobe bound to apoptotic EL-4 cells. $T_1$-weighted images (A) and $T_1$ relaxation time maps (B) from cell samples are shown. The $T_1$ relaxation rates ($1/T_1$) ($R_1$, mean ± SD) obtained from the maps are shown in (C). Apoptotic EL4 cells ($10^7$) were incubated at 20 °C, in HBS containing 2 mM $CaCl_2$, with increasing concentrations of the nanoprobe (0, 0.3, 1.7, 3.3, 8.3, 16.7, 33.3, 66.7 $\mu$M, clockwise) and then washed. Control tubes contained (a) apoptotic cells, (b) apoptotic cells that had been incubated with 16.7 $\mu$M active nanoprobe in HBS containing 10 mM EDTA, and (c) apoptotic cells that had been incubated with 16.7 $\mu$M of inactive nanoprobe in HBS containing 2 mM $CaCl_2$. The value of the $T_1$ relaxation rate (mean ± SD) for the latter control is displayed as a triangle in plot (C). The vertical scale in (B) represents $T_1$ relaxation time (0−3 s). (i) indicates a capillary tube containing HBS buffer, which was used as a reference.

Surface plasmon resonance (SPR) analysis of the binding of these complexes to PS-containing liposomes showed the active complexes to have dissociation constants in the nanomolar range (see Supporting Information, Table 1). The data for the [biotC2A]$_2$[Avidin-Gd] and [biot-(i)C2A]$_2$-[Avidin-Gd] complexes are shown in (Figure 2). This showed the active bivalvent complex to have a high affinity for PS ($K_d = 54 \pm 12$ nM, mean ± SD, $n = 3$) (Figure 2A), with negligible binding of its inactive counterpart (Figure 2B). A stoichiometry of 2 [biotC2A] to 1 [Avidin-Gd] molecule appeared to be optimal since there was minimal high-molecular-weight polymer formation, as determined by gel filtration chromatography (see Supporting Information, Table 1), and yet the reagent still had a high affinity for PS, in the nanomolar range.

Binding of the active bivalent nanoprobe to dead cells was assessed using flow cytometry (Figure 3). Cell death was induced in EL-4 murine lymphoma cells by incubating them for 16 h with 15 $\mu$M etoposide[17] (Eposin, Pharmachemie BV, Haarlem, The Netherlands). Binding of active or inactive bivalent complexes to apoptotic and necrotic cells was detected using NeutrAvidin (Pierce) conjugated to the fluorophore Alexa-350 (Molecular Probes, Invitrogen, Grand Island, NY). Necrosis was detected by co-staining the cells with propidium iodide (Sigma, St. Louis, MO). NeutrAvidin is a non-glycosylated derivative of avidin, which has a neutral isoelectric point and shows reduced nonspecific adsorption to cells and tissues when compared to avidin.[18] The Alexa-350 fluorescence is shown on axis FL2 and the propidium iodide fluorescence on axis FL1 in Figure 3. The active

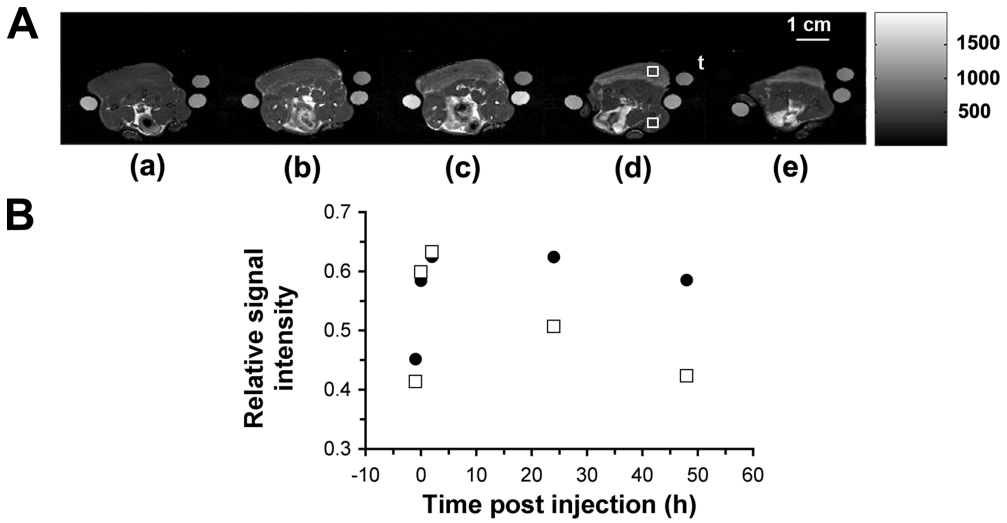


**Figure 6.** Axial $T_1$-weigthed spin−echo images (A) of a drug-treated murine EL-4 lymphoma tumor in an animal injected with the active nanoprobe [(biotC2A)$_2$(Avidin-Gd)]. A precontrast image (a) was acquired and then the nanoprobe administered i.v. (200 $\mu$L of a 0.5 mM solution in PBS). Post-contrast-agent injection images were acquired immediately after injection (b) and at 2 (c), 24 (d), and 48 h (e). Average relative signal intensities for tumor (closed symbols) and muscle tissue (open symbols) from the images in (A) are shown in (B). Regions of interest (ROI) were defined for the tumor (top square shown in (d)) and muscle tissue (bottom square in (d)). Signal intensity for both ROIs was normalized against a standard solution contained in a capillary tube placed adjacent to the tumor (t).

nanoprobe showed significant $Ca^{2+}$-dependent binding to early- and late-stage apoptotic cells (quadrant R4) and to necrotic cells (R2), with minimal binding to viable cells (R3 (iii), $+Ca^{2+}$, in Figure 3). In the absence of $Ca^{2+}$ there was negligible binding of the active nanoprobe, which was indistinguishable from that observed with the inactive nanoprobe in the presence or absence of $Ca^{2+}$ (compare parts A and B of Figure 3, $-Ca^{2+}$, and Figure 3B, $+Ca^{2+}$). The population of apoptotic cells ((ii) in Figure 3A) showed lower autofluorescence on the Alexa-350 axis (FL2), compared to the viable cell population (iii). This effect, which has been observed previously,[19] is thought to be due to poly(ADP-ribose)polymerase (PARP)-mediated depletion of NAD(H) levels in the apoptotic cells. NADH shows similar fluorescence absorption and emission maxima as the Alexa-350 fluorochrome. PARP, which uses $NAD^+$ as a substrate, is activated by DNA damage.[20] This population of apoptotic cells with lower autofluorescence bound Avidin-Gd-C2, and thus neutravidin-Alexa 350, in the presence of $Ca^{2+}$, resulting in an increase in its FL2 fluorescence (see Figure 3A, $+Ca^{2+}$).

The binding of different [biotC2A]$_n$[Avidin-Gd] complexes to apoptotic cells was assessed subsequently using MRI measurements of the relaxation rates ($1/T_1$, R1) of pellets of cells that had been incubated with the complexes and then washed. A two-step addition of biotC2A and [Avidin-Gd] (Figure 4(1)), at different molar ratios, was compared with a one-step addition (Figure 4(2)), in which the ratios of biotC2A to [Avidin-Gd] were in the range 0.8−3.0. The first of these approaches (two-step addition) did not yield significant binding of the complex, when compared with cells incubated with [Avidin-Gd] alone, which showed negligible binding (compare bar a with bar b and bar f with bar g in Figure 4). This was also noted previously, where it was shown that biotin-labeled C2A bound to the surface of apoptotic cells could not be bound by [Avidin-Gd] added subsequently, whereas biotin-labeled GST-C2A could be bound.[11] Presumably the smaller size of C2A renders the biotin inaccessible to avidin on the surface of the cell. However, the one-step addition of a single nanoprobe complex consistently produced an increase of the average relaxation rate (R1), that was up to 2.2-fold greater compared to the control (Figure 4(2,B)). The increase in R1 was proportional to the molar excess of biotC2A to [Avidin-Gd] (bars h−k in Figure 4(2)), suggesting that the larger, multivalent nanoprobes had increased affinity for the apoptotic cells, which was consistent with their increased affinity for PS observed in the SPR measurements (see Supporting Information, Table 1).

Binding of the bivalent nanoprobe [biotC2A]$_2$[Avidin-Gd] to apoptotic cells was further assessed over a wider range of concentrations of the complex (Figure 5). An increase in relaxation rate (R1) with nanoprobe concentration was observed, with partial saturation above a concentration of approximately 8 $\mu$M, corresponding to 3 nmol of the nanoprobe (Figure 5C). This increase was visible both on $T_1$-weighted images (Figure 5A) and on $T_1$ maps (Figure 5B). The relaxation rate produced by binding of an inactive bivalent nanoprobe ([biot-(i)C2A]$_2$[Avidin-Gd]), at a concentration of 17 $\mu$M (Figure 5C), was approximately 4-fold lower when compared to that produced by the active nanoprobe, at the same concentration. This further demonstrates the specificity of the active agent for binding to dying cells, which was also observed in the flow cytometry measurements.

To demonstrate that the agent was capable of accessing tumor cells *in vivo*, a female C57BL/6 mouse was injected subcutaneously in the flank, with $5 \times 10^6$ EL-4 cells. When the subcutaneous tumor volume reached ca. 1 cm$^3$, the animal was treated with a single intraperitoneal injection of etoposide (67 mg/kg) to induce tumor cell death.[12] Sixteen hours later, precontrast, $T_1$-weighted spin−echo MR images were ac-

quired (see Supporting Information). The nanoprobe was then administered intravenously (200 $\mu$L of a 0.5 mM solution in PBS) and post-contrast-agent injection images were obtained immediately after injection and at 2, 24, and 48 h. Figure 6 shows the accumulation of the nanoprobe in tumor tissue and clearance from the surrounding muscle tissue. Further work is required to demonstrate that the nanoprobe is detecting dying cells in the tumor.

We have described a paramagnetic nanoprobe that binds with high specificity and affinity to the PS exposed by dying cells and which thus could be used for the MRI detection of cell death in vivo. Since PS exposure results from all forms of cell death and since it is now recognized that all forms of cell death are important as early indicators of tumor responses to therapy, this makes this reagent particularly useful.[7,21] The nanoprobe, which can generate positive contrast, is sufficiently sensitive to be detected in $T_1$-weighted images. This is important since, unlike $T_1$ maps, these can be acquired relatively rapidly, do not require significant image processing, and are routinely acquired clinically. The use of avidin as a $Gd^{3+}$ carrier and its cross-linking to biotinylated C2A has two important advantages over direct conjugation of $Gd^{3+}$-chelates to C2A. First, the biotinylation of C2A does not change significantly its binding to PS, whereas we have shown that direct attachment of $Gd^{3+}$-chelates to C2A, or to a C2A-GST fusion protein, can significantly reduce their affinity for PS.[22] Avidin can carry considerably more $Gd^{3+}$ ions than C2A without loss of function. Second, the complex described is bivalent and therefore shows enhanced avidity compared to C2A alone. A problem with unmodified avidin is that it is immunogenic, and this could limit its application in human studies. However, extensive modification of the protein (e.g., PEGylation) can reduce dramatically its immunogenicity and increase its plasma half-life,[23,24] and it seems plausible that the extensively modified form of avidin used here may also have low immunogenicity, although this remains to be determined.

Introduction into the clinic of this or a similar agent, which is capable of detecting the early responses of tumors to treatment, may provide a useful alternative to FDG-PET assessments of tumor responses to treatment.

**Acknowledgment.** This work was supported by a grant from Cancer Research UK (CUK Grant C197/A3514).

**Supporting Information Available:** Detailed descriptions of Experimental Methods including protein expression, cleavage and purification, estimation of protein concentration, preparation of gadolinium-labeled avidin, preparation of [biotC2A]$_n$[Avidin-[Gd-DTPA]] and [biot-(i)C2A]$_n$[Avidin-[Gd-DTPA]] complexes, determination of gadolinium-labelling, surface plasmon resonance, cell culture and induction of apoptosis, flow cytometry, and MRI and a table listing properties of [biotC2A]$_n$[Avidin-Gd] complexes. This material is available free of charge via the Internet at http://pubs.acs.org.

## References

(1) Miller, A. B.; Hoogstraten, B.; Staquet, M.; Winkler, A. *Cancer* **1981**, *47*, 207−214.
(2) Therasse, P.; Arbuck, S.; Eisenhauer, E.; Wanders, J.; Kaplan, R.; Rubinstein, L.; Verweij, J.; Van Glabbeke, M.; Van Oosterom, A. T.; Christian, M.; Gwyther, S. G. *J. Natl. Cancer Inst.* **2000**, *92*, 205−216.
(3) Atri, M. *J. Clin. Oncol.* **2006**, *24*, 3299−3308.
(4) Juweid, M. E.; Cheson, B. *N. Engl. J. Med.* **2006**, *354*, 496−507.
(5) Haioun, C.; Itti, E.; Rahmouni, A.; Brice, P.; Rain, J. D.; Belhadj, K.; Gaulard, P.; Garderet, L.; Lepage, E.; Reyes, F.; Meignan, M. *Blood* **2005**, *106*, 1376−1381.
(6) Pottgen, C.; Levegrun, S.; Theegarten, D.; Marnitz, S.; Grehl, S.; Pink, R.; Eberhardt, W.; Stamatis, G.; Gauler, T.; Antoch, G.; Bockisch, A.; Stuschke, M. *Clin. Cancer Res.* **2006**, *12*, 97−106.
(7) Belhocine, T.; Steinmetz, N.; Hustinx, R.; Bartsch, P.; Jerusalem, G.; Seidel, L.; Rigo, P.; Green, A. *Clin. Cancer Res.* **2002**, *8*, 2766−2774.
(8) Kartachova, M.; Haas, R. L.; Olmos, R. A.; Hoebers, F. J.; Van Zandwijk, N.; Verheij, M. *Radiother. Oncol.* **2004**, *72*, 333−339.
(9) Neves, A. A.; Brindle, K. *Biochim. Biophys. Acta* **2006**, *1766*, 242−261.
(10) Kettunen, M. I.; Brindle, K. M. *Prog. Nucl. Magn. Reson. Spectrosc.* **2005**, *47*, 175−185.
(11) Jung, H.; Kettunen, M.; Davletov, B.; Brindle, K. M. *Bioconjugate Chem.* **2004**, *15*, 983−987.
(12) Zhao, M.; Beauregard, D.; Loizou, L.; Davletov, B.; Brindle, K. *Nat. Med.* **2001**, *7*, 1241−1244.
(13) Kobayashi, H.; Kawamoto, S.; Jo, S. K.; Bryant, H. L., Jr.; Brechbiel, M. W.; Star, R. A. *Bioconjugate Chem.* **2003**, *14*, 388−394.
(14) Green, N. M. *Biochem. J.* **1965**, *94*, 23C−24C.
(15) Bryant, L. J.; Brechbiel, M.; Wu, C.; Bulte, J. W.; Herynek, V.; Frank, J. *J. Magn. Reson. Imaging* **1999**, *9*, 348−352.
(16) Langereis, S.; De Lussanet, Q. G.; Van Genderen, M. H.; Meijer, E.; Beets-Tan, R. G.; Griffioen, A.; Van Engelshoven, J. M.; Backes, W. *NMR Biomed.* **2006**, *19*, 133−141.
(17) Schmitz, J. E.; Kettunen, M.; Hu, D.; Brindle, K. M. *Magn. Reson. Med.* **2005**, *54*, 43−50.
(18) Hiller, Y.; Gershoni, J.; Bayer, E. A.; Wilchek, M. *Biochem. J.* **1987**, *248*, 167−171.
(19) Poot, M.; Pierce, R. H. *Cytometry* **1999**, *35*, 311−317.
(20) Du, L.; Zhang, X.; Han, Y.; Burke, N.; Kochanek, P.; Watkins, S. C.; Graham, S.; Carcillo, J.; Szabo, C.; Clark, R. S. *J. Biol. Chem.* **2003**, *278*, 18426−18433.
(21) Corsten, M. F.; Hofstra, L.; Narula, J.; Reutelingsperger, C. *Cancer Res.* **2006**, *66*, 1255−1260.
(22) Krishnan, A.; Neves, A.; Kettunen, M.; Hu, D.-E.; De Backer, M.; Brindle, K. M. *Proc. Int. Soc. Mag. Reson. Med.* **2006**, *14*, 1838.
(23) Chinol, M.; Casalini, P.; Maggiolo, M.; Canevari, S.; Omodeo, E. S.; Caliceti, P.; Veronese, F. M.; Cremonesi, M.; Chiolerio, F.; Nardone, E.; Siccardi, A. G.; Paganelli, G. *Br. J. Cancer* **1998**, *78*, 189−197.
(24) Caliceti, P.; Chinol, M.; Roldo, M.; Veronese, F.; Semenzato, A.; Salmaso, S.; Paganelli, G. *J. Controlled Release* **2002**, *83*, 97−108.

NL070126V